

# Analyst

Accepted Manuscript

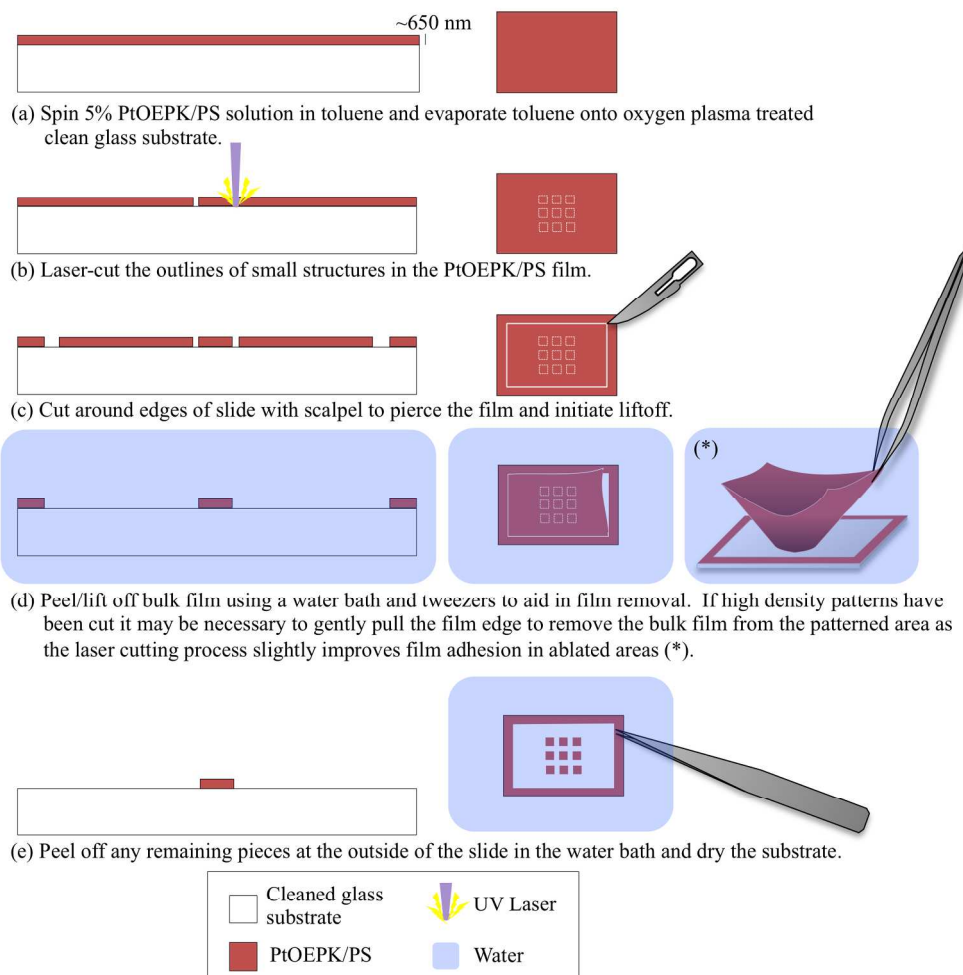


This is an *Accepted Manuscript*, which has been through the Royal Society of Chemistry peer review process and has been accepted for publication.

*Accepted Manuscripts* are published online shortly after acceptance, before technical editing, formatting and proof reading. Using this free service, authors can make their results available to the community, in citable form, before we publish the edited article. We will replace this *Accepted Manuscript* with the edited and formatted *Advance Article* as soon as it is available.

You can find more information about *Accepted Manuscripts* in the [Information for Authors](#).

Please note that technical editing may introduce minor changes to the text and/or graphics, which may alter content. The journal's standard [Terms & Conditions](#) and the [Ethical guidelines](#) still apply. In no event shall the Royal Society of Chemistry be held responsible for any errors or omissions in this *Accepted Manuscript* or any consequences arising from the use of any information it contains.



Fabrication process flow for the new oxygen sensor fabrication and patterning process.

# Fabrication and laser patterning of polystyrene optical oxygen sensor films for lab-on-a-chip applications

Cite this: DOI: 10.1039/x0xx00000x

Received 00th January 2012,  
Accepted 00th January 2012

DOI: 10.1039/x0xx00000x

[www.rsc.org/](http://www.rsc.org/)

S. M. Grist,\* N. Oyunerdene, J. Flueckiger, J. Kim, P. C. Wong, L. Chrostowski, and K. C. Cheung,

We present a novel and simple method for patterning oxygen-sensitive polystyrene thin films and demonstrate its potential for integration with microfluidic lab-on-a-chip devices. Optical oxygen sensing films composed of polystyrene with an embedded luminescent oxygen-sensitive dye present a convenient option for the measurement of oxygen levels in microfluidic and lab-on-a-chip devices; however, patterning and integrating the films with poly(dimethylsiloxane) (PDMS) microfluidic devices has proven difficult due to a residue after dry etch patterning that inhibits subsequent PDMS bonding. Our new method uses mask-less laser ablation by a commercial laser ablation system to define the outline of the structures and subsequent bulk film removal by aqueous lift-off. Because the bulk film is peeled or lifted off of the substrate rather than etched, the process is compatible with standard PDMS plasma bonding. We used ToF-SIMS analysis to investigate how laser ablation facilitates this fabrication process as well as why dry etching polystyrene inhibits PDMS plasma bonding. The results of this analysis showed evidence of chemical species formed during the laser ablation and dry etching processes that can produce these effects. Our new method's mask-less nature, simplicity, speed, and compatibility with PDMS bonding make it ideally suited for single-use lab-on-a-chip applications. To demonstrate the method's compatibility with PDMS microfluidics, we also present a demonstration of the sensors' integration into a microfluidic oxygen gradient generator device.

## Introduction

### Optical oxygen sensing in lab-on-a-chip devices

Oxygen is of great importance in many of the biological and chemical systems modelled in lab-on-a-chip devices. As such, the integration of a reliable oxygen sensing mechanism into lab-on-a-chip devices is of great interest<sup>1</sup>. Optical, luminescence-based oxygen sensors present an attractive option for sensing oxygen levels inside microfluidic devices because they do not consume oxygen, are easily miniaturized, and are read out optically and thus do not require physical contact between the sensing material and the readout system<sup>1-3</sup>.

These sensors operate on the principle of reversible luminescence quenching, in which both the luminescence intensity and lifetime are quenched by the presence of oxygen. In the ideal case neglecting the effects of static quenching and system inhomogeneities, this quenching can be modelled by the Stern-Volmer equations<sup>4, 5</sup>:

$$\frac{I_0}{I} = 1 + K_{SV}pO_2, \quad (1)$$

$$\frac{\tau_0}{\tau} = 1 + K_{SV}pO_2,$$

$$K_{SV} = k_Q\tau_0,$$

where  $I_0$  and  $I$  are the emission intensities in the absence of oxygen and at oxygen partial pressure  $pO_2$ , respectively,  $\tau_0$  and  $\tau$  are the luminescence lifetimes at zero oxygen and  $pO_2$ , respectively, and  $K_{SV}$  is the Stern-Volmer quenching constant, which is dependent on the unquenched fluorescence lifetime and the diffusion-controlled bimolecular rate constant  $k_Q$ .

Optical oxygen sensors can be interrogated by measuring either the luminescence intensity or lifetime. Although lifetime-based sensing is more robust to inhomogeneities in sensor film thickness, measurement setup, and dye distribution<sup>6, 7</sup>, the measurement setup for intensity-based sensing is much easier and less expensive to implement, as it requires only a

1 fluorescence microscope. For this reason, intensity-based  
2 sensing is attractive as a proof-of-concept sensing modality.  
3 Ratiometric sensing using a reference dye to account for some  
4 of the system inhomogeneities is a good compromise between  
5 the two methods, providing more robust measurements without  
6 a significant increase in the complexity of the measurement  
7 setup<sup>8-11</sup>.

### 9 **Optical oxygen sensor fabrication**

10 Luminescent sensing molecules can be encapsulated in polymer  
11 or sol-gel matrices<sup>12</sup> in order to form an oxygen-sensitive film  
12 that may be integrated with microfluidics. One commonly-used  
13 sensor film is platinum octaethylporphyrin ketone (PtOEPK)  
14 dye encapsulated in a polystyrene (PS) matrix<sup>13</sup>; this type of  
15 film has been found to have good oxygen sensitivity and  
16 photostability. To make PtOEPK/PS films, the PtOEPK and  
17 polystyrene can be dissolved in a solvent such as toluene or  
18 chloroform to yield sensor cocktails. The sensor cocktail can  
19 then be directly dispensed to form patches (via pipetting)<sup>14-16</sup> or  
20 spin- or knife-coated<sup>11, 17</sup> to form sensor films on glass  
21 substrates for integration with microfluidic devices. Because  
22 the measured luminescence intensity of the sensing film is  
23 dependent on film thickness, uniform spin- or knife-coated  
24 polymer sensor films are ideal for intensity-based or ratiometric  
25 sensing. Thin, flat glass substrates are commonly used for  
26 microfluidic devices and permit high-resolution microscopic  
27 imaging of the device; as such, this paper focuses on the  
28 development of a sensor patterning method on glass substrates.

29 There are four potential complications of using the spin-coating  
30 method for microfluidic devices without patterning the film.  
31 Firstly, non-standard bonding methods such as the use of  
32 silanes<sup>18, 19</sup> or carefully controlled air plasma parameters<sup>20</sup> must  
33 be used to facilitate the bonding of polystyrene with  
34 poly(dimethylsiloxane) (PDMS) devices, potentially  
35 complicating the fabrication process. The second issue is that  
36 polystyrene films adhere poorly to glass, greatly limiting the  
37 mechanical stability of the microfluidic device if PS-PDMS  
38 bonding is achieved. Thirdly, although the films are  
39 transparent, the presence of a sensor film at the bottom of the  
40 channel could affect sensitive imaging of other components of  
41 the microfluidic system. High-resolution imaging of  
42 microfluidic devices is required in certain applications such as  
43 microfluidic cell culture, and un-patterned sensor films can  
44 interfere with this. Slightly uneven sensor films could  
45 contribute to scattering effects degrading image quality during  
46 confocal microscopy, and the luminescent properties of the  
47 sensor film could interfere with fluorescent signals (ratiometric  
48 sensors employing multiple sensing dyes would present the  
49 highest likelihood of this interference). Finally, adherent cell  
50 cultures may be used for biological assays, and a treated glass  
51 substrate may be preferable for this application rather than the  
52 sensor film containing dyes (especially for comparison with  
53 other glass cell culture platforms such as high optical quality  
54 glass-bottom well plates). Although the bonding and stability  
55 problems can be addressed by the use of a spin-coated PDMS

film on top of the sensing layer<sup>11</sup>, patterning the films is  
necessary to address all four issues with microfluidic  
integration.

Alternative sensor types involve hot embossing PtOEPK/PS  
films to generate microwells for cell culture<sup>21</sup>, or incorporating  
oxygen-sensitive indicator molecules directly into photoresist  
or photopatternable PDMS matrices to form inherently  
photopatternable films<sup>22, 23</sup>. The hot-embossed microwells  
form an attractive platform for cell culture, were demonstrated  
as compatible with confocal microscopy, and are compatible  
with PDMS microfluidics via the bonding methods discussed  
above; however, the hot embossing process does not yield film-  
less regions in the substrate. As such, the sensor film would  
still need to be imaged through and thus could interfere with  
imaging, particularly if ratiometric sensing were used.  
Although the photoresist-based films were tested for cell  
adherence and short-term culture, photoresists are often not  
biocompatible so these types of films may not be suitable for  
many lab-on-a-chip applications involving long-term cell  
culture.

While PtOEPK/PS films can be spin-cast onto glass substrates  
to form uniform sensor films with good intensity sensing  
characteristics, patterning of the films for subsequent  
integration into microfluidics can be difficult because the  
solvents and strippers of many common photoresists can attack  
the polystyrene matrix. To mitigate this problem, dry etching  
methods employing a pinhole-free metal etch mask<sup>24, 25</sup> and  
removable PDMS 'stamps'<sup>17</sup> have been proposed. We have  
also previously demonstrated a non-photolithographic dry etch  
method utilizing a water-soluble polyvinyl alcohol (PVA) etch  
mask<sup>26</sup>. Alternatively, new resists compatible with the  
underlying film could potentially also be used to directly  
address the photoresist compatibility issue. All of these  
methods may be confounded by the dry etch itself, however, as  
we have found that residue on the glass slides after dry etching  
of the polystyrene inhibits subsequent plasma bonding of  
PDMS, which complicates the patterned sensors' use in  
microfluidics. We tried various models of oxygen plasma  
etchers (Technics PE-II, Trion PECVD, and Sentech Etchlab  
200 RIE) but were unable to reliably bond PDMS to  
previously-etched substrates in all cases. Evidence of a residue  
left behind after oxygen plasma etching of other polymers has  
also been reported in other applications<sup>27, 28</sup>. To overcome this  
challenge, we devised a simple and mask-less method for the  
patterning of polystyrene optical oxygen sensor films in which  
the bulk film is peeled/lifted off rather than etched. This  
process is facilitated by the poor adhesion between the glass  
and PtOEPK/PS film, as discussed above.

### 56 **Laser patterning of polystyrene**

Our method patterns the polystyrene film containing the  
oxygen-sensitive dye using a commercial laser cutter system.  
Laser ablation of polystyrene has been previously found to be a  
thermal and photothermal dissociative process that 'unzips' the

1 polymers into monomer styrene<sup>29, 30</sup>. We use laser ablation to  
2 selectively remove polystyrene from pattern edges, separating  
3 desired patterns from the film bulk. Because the laser is only  
4 used in small regions compared to the large substrate areas  
5 affected by plasma etch processes, any residue left behind after  
6 laser ablation does not impact subsequent PDMS bonding.  
7

8 This paper presents our novel sensor patterning fabrication  
9 process, as well as the sensing performance and  
10 characterization of the patterned sensors. We characterized the  
11 physical structure of the patterned sensor films using bright-  
12 field, fluorescence, and atomic force microscopy (AFM). We  
13 also investigated the chemical residues left on the glass after  
14 laser-cutting, oxygen plasma dry etching, and bulk film lift-  
15 off/peeling in order to understand the mechanism by which this  
16 method operates as well as to understand why polystyrene dry  
17 etch processes inhibit subsequent PDMS bonding. Finally, we  
18 demonstrate the compatibility of our fabrication process with  
19 PDMS microfluidic devices by integrating the patterned sensors  
20 with a microfluidic oxygen gradient generator device and  
21 measuring *in situ* oxygen gradients.  
22  
23

## 24 Methods

25 The phosphorescent oxygen sensor films were fabricated by  
26 spin coating, patterned by mask-less laser ablation, and  
27 integrated with a microfluidic device patterned with standard  
28 soft lithography. This section details the methods used to  
29 fabricate the sensors, as well as the methods by which they  
30 were tested and characterized, including their microfluidic  
31 integration.  
32

## 33 Materials

34 Platinum (II) octaethylporphyrin ketone (PtOEPK) (Frontier  
35 Scientific), polystyrene pellets (MW 280 000, Sigma Aldrich)  
36 and toluene (CHROMASOLV<sup>®</sup> 99.9%, Sigma Aldrich) were  
37 used to fabricate the sensor films. Soda-lime glass slides of  
38 size 50 x 75 x 1 mm (Fisher Scientific) were used as the glass  
39 substrates. Dow Corning Sylgard 184 PDMS was used for the  
40 microfluidic devices (Paisley Products of Canada).  
41

## 42 Sensor fabrication

43 The fabrication process flow diagram is presented in Figure 1.  
44 PtOEPK (1 mg/mL) dissolved in a solution of polystyrene (PS)  
45 in toluene (5% w/w) is first spin cast onto a soda-lime glass  
46 substrate after preparing the substrate with a 5 minute oxygen  
47 plasma exposure (Technics Planar Etch II, at a pressure of 400  
48 mTorr and a power of 180 W) to improve polystyrene adhesion  
49 (Figure 1 (a)). The films were measured (after solvent  
50 evaporation and a 5 minute bake at 100°C) to be approximately  
51 650 nm in thickness using non-contact AFM measurements  
52 (Nanosurf easyScan 2). A Quiklaze-50 ST2 Nd:YAG laser  
53 system (ESI, Portland, Oregon) outfitted with a 50x  
54 magnification objective and x-y translation stage (maximum  
55 translation distance of 50 mm in each direction, precision of 1  
56  $\mu\text{m}$ <sup>31</sup>, variable laser aperture size of 2-50  $\mu\text{m}$ ) is then used to

trace around the edges of final patterns and ablate the  
polystyrene film (b). The sample was placed on a silicon wafer  
during patterning to act as a non-transparent substrate. It is  
important to completely cut through the polymer film to  
separate the desired patterns from the bulk in order to prevent  
patterned structures from lifting off with the bulk film. We  
found that the UV3 (355 nm) high power setting (5.1 W/ $\mu\text{m}^2$ )<sup>32</sup>  
at a 50 Hz frequency with a 40  $\mu\text{m/s}$  scan speed yielded  
excellent results after two passes for our 650 nm film thickness.  
Although most of the film was ablated after a single pass,  
residue was visible in some regions that connected the patterns  
and the bulk film; two passes were used in order to ensure that  
the patterns were completely separated from the bulk. After  
two passes, the patterns were completely separated from the  
bulk but slight residue remains in the laser cut regions, as  
shown in Figure 2 (b) and the AFM measurements. A 5  $\mu\text{m}$  x 5  
 $\mu\text{m}$  square aperture was used for the patterned sensor films  
presented in this work.

After completion of the laser tracing, the bulk film around the  
patterns is removed by aqueous lift-off/peeling; a water bath  
aids in this process (depicted in Figure 1 (c-d)). We find that  
tracing around the edge of the glass slide with a scalpel to  
penetrate the film and start the lift-off process prior to placing  
the sample in the water bath helps ensure good results. We find  
that the scalpel tugs at the film during cutting, locally  
delaminating it near the cut and allowing the water to start  
penetrating under the film (whereas the laser tends to seal the  
cut edges to the substrate).

During the peeling/lift-off process we find that the film is easy  
to remove in one or two large pieces, leaving behind the  
isolated patterns and removing the need to touch the film or  
substrate in areas close to the patterns of interest. To lift off the  
film, the glass slide is first placed on the water surface; the  
polystyrene-coated 1 mm thick soda-lime glass slides will sit  
atop the water surface. The slide corners are then very gently  
pushed down; if the slide is pushed very slowly to the point  
where the water meets the scalpel-cut interface, the water  
slowly seeps underneath the scalpel-cut film, peeling off the  
film bulk as the sample sinks. The bulk film is often left  
floating atop the water bath after the sample sinks to the  
bottom. If the sample stops sinking or pulls the film below the  
surface, we find that the film edge (already lifted by the water)  
may be gently pulled with tweezers to lift it from the substrate  
without touching the substrate near the patterns. We have  
found this necessary when patterning high-density patterns,  
indicating a small improvement in film adhesion at the  
patterned interfaces. This process is depicted in Figure 1 (d)(\*).  
After removal of the bulk of the film close to the sensors, the  
edges of the film outside of the scalpel line may be removed by  
pulling with tweezers in the water bath.

## ARTICLE

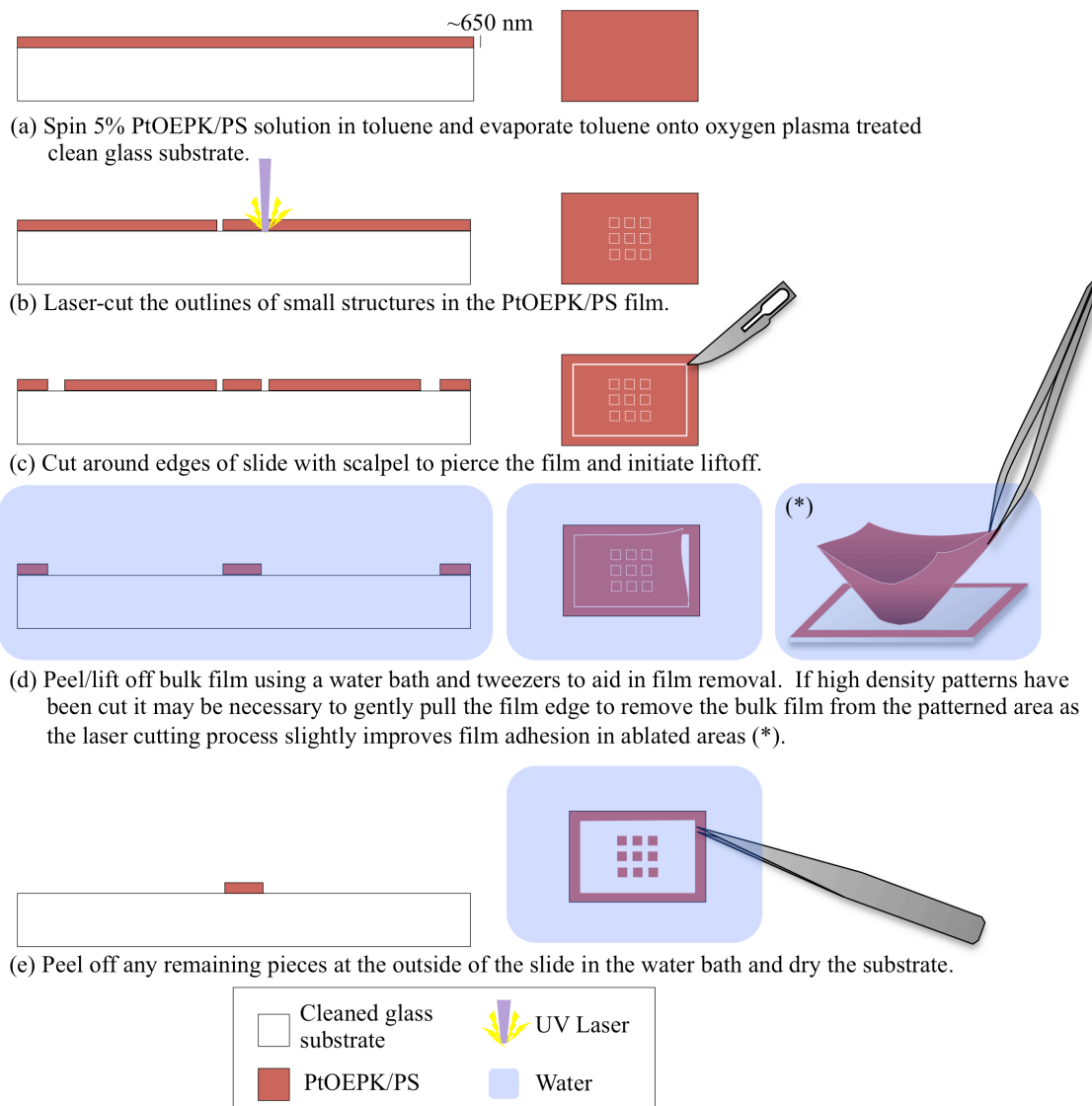


Figure 1. Fabrication process flow diagram for the oxygen sensor fabrication and patterning process.

After the bulk film has been removed, the patterned sensors are gently dried with a nitrogen gun, baked on a hotplate for 10 minutes at 100°C, and cooled prior to storage or microfluidic integration.

#### Microfluidic fabrication and sensor integration

To demonstrate compatibility with PDMS microfluidics, we integrated the patterned sensors into a microfluidic device. The device we chose for this purpose was an oxygen gradient generator with a large central chamber and parallel separated

400  $\mu\text{m}$  gas control channels, similar to previously demonstrated oxygen control microfluidic devices<sup>33-35</sup>. Fluid is supplied to the 3 mm central chamber at a slow flow rate (0.5-1  $\mu\text{L}/\text{min}$ , velocity of 9-18  $\mu\text{m}/\text{s}$ ) while the gas control side channels control the oxygen levels in the central chamber. Because one potential disadvantage of gradient generator designs employing pressurized gas control channels is the possibility for bubbles to develop inside the fluid channels due to the high gas permeability of PDMS<sup>34</sup>, we also integrate narrow (100  $\mu\text{m}$ ) fluid channels perfused with fluid at a rate of

0.25  $\mu\text{L}/\text{min}$  between the gas control channels and microfluidic chamber in an effort to remove any bubbles. This use of fluidic side channels is similar to one previously used for a multilayer oxygenator system<sup>36</sup>.

The microfluidic channels were patterned in PDMS by standard soft lithography using an intermediate polyurethane replicate of the original wafer of SU-8 3050 photoresist on silicon (photolithographically patterned to form channels 360  $\mu\text{m}$  in height). Inlets and outlets are bored using a 0.5 mm punch (Harris Uni-Core) before bonding with the glass substrate containing the patterned sensors.

Permanent plasma bonding was used to enclose the microfluidic channels as the gaseous and fluidic pressures in the device can exceed the maximum pressure allowed for reversibly bonded PDMS (approximately 5 psi, as reported by Martin *et al.*<sup>37</sup>). To bond the device, the PDMS microfluidic channels and glass substrate around the patterned polystyrene sensors were exposed to air plasma for one minute and then brought into contact. Devices were left overnight in a 65°C oven to complete the bonding between the PDMS and lifted-off glass regions. Final devices were connected to Tygon® microbore tubing (Cole-Parmer) with blunt 22 gauge needles (Nordson EFD) after sensor integration.

#### Sensor characterization

**MICROSCOPY** After patterning, the sensors were characterized under bright-field and fluorescence microscopy to verify the lift-off fidelity. To obtain these microscope images, a Nikon TE-2000-U microscope was equipped with a bandpass excitation filter (Omega Optical 400AF30), long-pass dichroic mirror (Omega Optical 475DCLP), and long-pass emission filter (Omega Optical 700ALP), mercury arc fluorescence excitation lamp (Nikon Intensilight® C-HGFI) and colour camera (Qimaging Retiga EXi). The fluorescence microscopy filters were chosen to provide and measure PtOEPK dye excitation and emission wavelengths of 398 nm and 759 nm<sup>13</sup>, respectively. The 3-D pattern geometries and the morphology of the laser cut interface were characterized with an AFM (Nanosurf easyScan 2) operating in non-contact mode.

Test structures were also patterned to investigate the limitations on the patterning process in terms of pattern spacing aspect ratio (the maximum length/width ratio facilitating lift-off, where the length was ablated with the laser to separate the pattern and the width was connected to the bulk film). We have observed slightly improved film adhesion near laser cut regions of the film, as evidenced by the need to use tweezers to lift off the bulk film near high density patterns as illustrated in Figure 1 (d)(\*); we anticipated that at some aspect ratio (the length of ablated lines divided by the spacing between them) the improvement in adhesion provided by the laser cutting process would cause the film between the cut lines to tear, remaining attached to the substrate and causing the patterning process to fail.

To find the maximum aspect ratio resolvable with this patterning process, we patterned U-shaped ‘flap’ structures (rectangles with only three sides cut) of varying aspect ratios (the length of the long side of the rectangles divided by the length of the shorter side containing the un-cut edge). More details regarding these flap structures are presented in Figure S1 of the electronic supplementary information. Flaps with aspect ratios of 1, 2, 4, 10, 20, 40, 100, 200, and 500 were patterned, subjected to the lift-off process, and examined after lift-off to determine whether the flap had lifted off with the bulk or if it had torn at the un-cut edge, leaving behind a rectangle. The flap widths (short side) for the aspect ratios of 1, 2, 4, 10, 20, 40, and 100 were 50  $\mu\text{m}$ , while those for the aspect ratios of 200 and 500 were 25  $\mu\text{m}$  and 10  $\mu\text{m}$ , respectively.

**TOF-SIMS** In order to understand why the patterned structures do not lift off with the bulk film as well as to investigate why PDMS bonding is inhibited by dry etch processes of polystyrene, Time-of-Flight Secondary Ion Mass Spectrometry (ToF-SIMS) analysis was performed using a PHI TRIFT V nanoToF-SIMS spectrometer (Physical Electronics PHI, Inc.). A pulsed primary 30 keV Au<sup>+</sup> ion beam was raster scanned over a 400  $\mu\text{m}$   $\times$  400  $\mu\text{m}$  area. To ensure static analysis conditions, the total ion dose per spectrum was controlled to  $<1.3 \times 10^{12}$  ions/cm<sup>2</sup>. For one sample (the laser cut patterned sample), a mosaic ion image was acquired, wherein the stage was moved and the raster scanned sub-areas were stitched together to examine a larger, approximately 3.2 mm x 3.2 mm area.

A control sample as well as laser-cut and plasma etched polystyrene samples were prepared using processing steps similar to those used to pattern the sensor films, except the oxygen-sensitive dye was not added to the film. For a ‘degassed glass’ control as well as a first step for all other samples, soda-lime glass slides were degassed with solvent rinses (acetone, isopropanol, and deionized water) and dehydration baked for 10 minutes at 100°C.

For the polystyrene samples, the soda-lime substrates were first degassed as above and then oxygen plasma-etched in a Technics Planar Etch II system at a pressure of 400 mTorr and a power of 180 W, for 5 minutes. Immediately following this plasma etch step, a 2% (w/w) solution of polystyrene in toluene (using the same constituents as used for the oxygen-sensitive films above, except without the PtOEPK) was pipetted onto the glass substrates and allowed to evaporate for approximately 10 minutes before baking at 100°C again for 10 minutes. Profilometry (Dektak 150) measurements indicated that this deposition yielded a film approximately 1.2  $\mu\text{m}$  in thickness.

One of the polystyrene-coated samples was then oxygen plasma etched (Technics Planar Etch II) at a pressure of 400 mTorr and a power of 180 W for 10 minutes to mimic the removal of the polystyrene film in standard dry etch patterning processes.

Another polystyrene-coated sample was patterned using our laser cutting patterning process (laser ablation with the Quiklaze-50 ST2 followed by aqueous lift-off of the bulk film and drying with nitrogen) to generate a 1 mm x 1 mm polystyrene square. The 355 nm UV3 beam at 100% power intensity with two passes at a scan speed of 40  $\mu\text{m/s}$  was again used for this pattern; however, the full beam aperture (50  $\mu\text{m}$  x 50  $\mu\text{m}$ ) was used to yield more laser-cut surface area per pass for ease of analysis. The lifted off, polystyrene-coated, and laser ablated areas of this sample were all analysed separately and compared.

### Sensor calibration

To ensure that the sensor patterning process did not damage the sensors' sensing abilities, we calibrated the sensors to measure both gaseous and dissolved oxygen levels. For the gaseous sensor calibration, patterned sensors with bonded microfluidic devices were enclosed in a stage-top incubator chamber (Live Cell Instrument Chamlide) atop the same microscope setup used to acquire the fluorescence microscope images of the patterned sensors. A custom gas mixing system employing a commercial reference oxygen sensor (Presens) supplied 0%, 10%, and 20% oxygen to the setup. The chamber, gas control, and central microfluidic chamber were flushed with these gases for 15 minutes prior to acquiring fluorescence images of the three sensor patches in the field of view. The experiment was repeated three times for a total  $N=9$ , and the averaged intensities of the sensor patches were then fitted to the Stern-Volmer equation to obtain the sensors' calibration constants.

To obtain the fluidic sensor calibration constants, the patterned sensors and integrated microfluidics were enclosed in the same chamber as used for the gaseous calibration. To obtain the deoxygenated sensor intensities  $I_0$ , the oxygen control channels and chamber were flushed with 0% oxygen for 3 hours prior to acquiring images to ensure complete deoxygenation. The oxygen control channels and chamber were then flushed with 10% and 20% oxygen for 30 minutes each prior to acquiring fluorescence images of the sensor patches. Additionally, distilled water bubbled with nitrogen, air, and oxygen was supplied to the central microfluidic chamber. Fluid flow in this central chamber was maintained at a rate of 10 (for the first two experiments) and 100  $\mu\text{L/min}$  (for the final experiment), withdrawn with a syringe pump (kdScientific).

### Demonstration of microfluidic compatibility

As a final test, we integrated the sensors into the microfluidic oxygen gradient generator and measured oxygen gradients in a fluidic environment in order to demonstrate the patterning process's compatibility with microfluidic integration. To do this, the sensors and integrated microfluidics were again enclosed in the same chamber as used for the sensor calibration. Gaseous nitrogen was supplied to the ambient environment in the chamber, while gaseous oxygen and nitrogen were supplied to the microfluidic gas control channels. Oxygen and nitrogen were chosen as the control gases in order to demonstrate the full range of the sensor response. Distilled water flow in the

innermost, yellow main channel was maintained with a syringe pump at a rate of 0.5  $\mu\text{L/min}$ , while that in the middle, red bubble removal channels was maintained at 0.25  $\mu\text{L/min}$ .

Fluorescence microscope images were acquired and the fluidic calibration data were used to convert the image phosphorescence intensities into a map of the oxygen gradient in the device by the Stern Volmer equation (Equation 1). The device was immersed in fluid and left for three days with constant gas and fluid perfusion to the microfluidic channels in order to investigate the stability of the sensor adhesion to the glass substrate as well as the PDMS-glass bonding stability.

## Results

### Laser ablation and liftoff gives high pattern fidelity and integrability with PDMS devices

**MICROSCOPY CHARACTERIZATION** The patterned sensors were characterized with fluorescence and bright-field microscopy to verify pattern fidelity after lift-off; these results are presented in Figure 2.

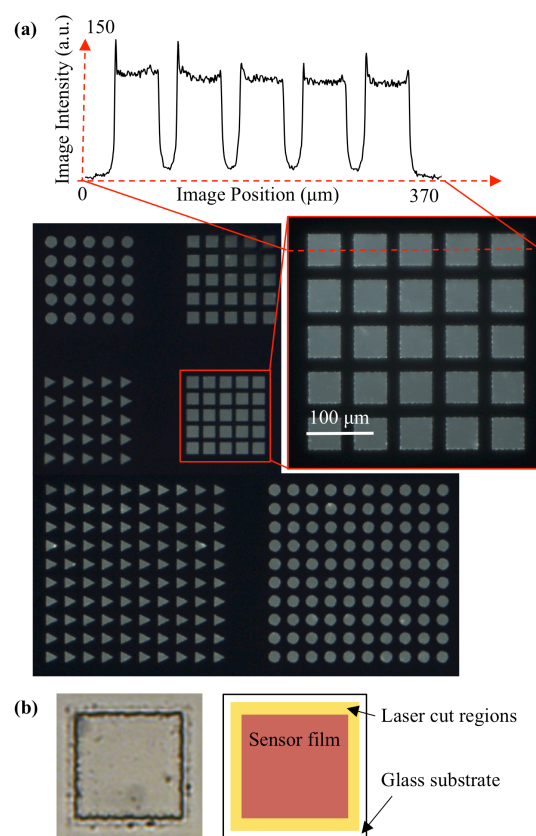


Figure 2. (a) Phosphorescence intensity images of the patterned sensor films, showing arrays of 50  $\mu\text{m}$  squares, circles, and triangles on a pitch of 75  $\mu\text{m}$  (except the lower array of squares and inset, on a pitch of 65  $\mu\text{m}$ ). An intensity cross-section of the array of squares is also presented. The peaks at pattern edges are likely due to redeposition during the laser ablation. As this effect is confined to the pattern edges we have eliminated any effects on the measurements by using a slightly smaller region of the sensor image for oxygen calculations. (b) Bright-field image of one of the arrays of squares in the patterned array, as well as a diagram indicating the different regions (sensor film, laser ablation line showing the residue remaining after laser cutting, and glass substrate) within it.

Phosphorescence intensity images of the patterned sensor films are presented in Figure 2 (a); we successfully demonstrated the patterning of 5x5 and 10x10 arrays of 50  $\mu\text{m}$  squares, circles, and triangles on pitches of 65 and 75  $\mu\text{m}$ . An intensity cross-section of the patterned square sensor array shows fairly uniform intensity characteristics across sensors along with evidence of redeposition (intensity peaks) at pattern edges from the laser ablation process. These intensity peaks at pattern edges were removed from our measurements by choosing a sensor sub-region slightly smaller than the full sensor size during our image analysis. Figure 2 (b) presents a bright-field image of a patterned sensor film along with a diagram indicating the different regions shown (sensor film, laser ablation line showing the residue remaining after laser cutting, and glass substrate). Figure 2 (b) shows that visible residue remains on the substrate in the laser ablated regions, although the patterned portions of the film were completely separated from the bulk to facilitate lift-off.

Although this new fabrication method can only be used to form simple patterns (all of the polystyrene areas to be removed must be connected), these types of patterns are sufficient for most lab on a chip oxygen sensing applications.

AFM images of patterned sensing squares as well as the flap structures are presented in Figure 3. We observe residue in the laser-cut areas both before and after lift-off, as well as a small increase in thickness of the polystyrene film around the structure edges, which could be evidence of redeposition. These data show a steady decrease in thickness near the laser-cut lines; Figure S2 of the electronic supplementary information presents cross-sectional AFM data examining this interface and comparing it with a scalpel-cut interface. We believe that the scalpel cutting process slightly delaminates the polystyrene film near the cut interface, while the laser cutting process is able to separate the patterned structures from the bulk without causing this delamination. Small amounts of re-deposition or melting near the glass side of the laser cut interface could also help seal the pattern edges to the substrate. The slight delamination caused by the scalpel cutting process likely permits the water to penetrate under the film, lifting it off of the substrate. In contrast, there is no such delamination at the laser cut interface, allowing the laser cut structures to remain attached to the substrate and facilitating the patterning process. Cross-sectional AFM profiles of a laser-cut and scalpel-cut interface are presented in Figure S2 of the electronic supplementary information.

The AFM results also indicate that the substrate in the lifted off areas appears to remain quite clean; mean film thicknesses and roughness calculations are presented in Figure S3 of the electronic supplementary information.

After bulk film lift-off, we examined the area containing the flap structures for the minimum spacing analysis using bright-field and fluorescence microscopy. The aspect ratio of the

structure needed to be very high ( $>100$ ) in order for the flap to tear across the un-cut edge and remain on the substrate; this indicates that very high aspect ratios of pattern spacing can be successfully patterned and lifted off with this process. It also indicates that the improvement in film adhesion provided by the laser cut process, although sufficient for patterning and microfluidic integration, is small in comparison to the strength of the 650 nm thick film. Full results of the minimum spacing investigation as well as the details regarding the flap designs patterned are presented in Figure S1 and the surrounding section of the electronic supplementary information.

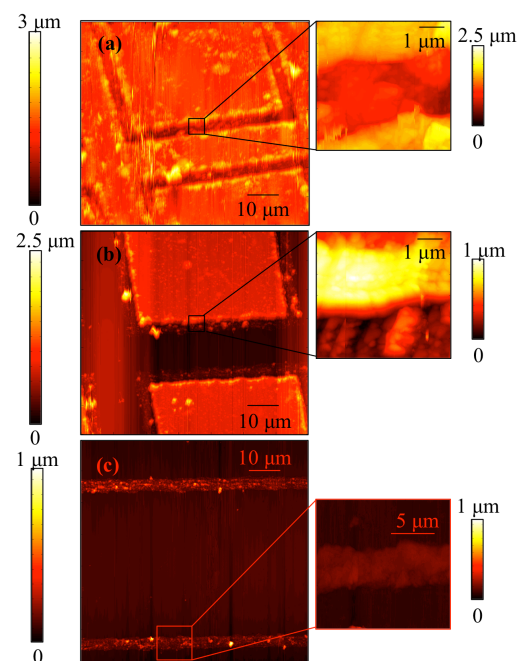


Figure 3. Non-contact AFM images of patterned sensing squares before (a) and after (b) bulk film removal, showing overall morphology as well as edge detail. (c) depicts the laser cut area alone after bulk film removal of the incompletely outlined flap structures (no patterned film remaining).

**TOF-SIMS CHARACTERIZATION** Analysis of the laser-cut and plasma etched polystyrene samples and comparison with the degreased glass control showed that three main chemical species were formed in these processes that could contribute to the results we observed. It was found that plasma etched polystyrene films left residual chemical species giving the fragment  $[\text{C}_8\text{H}_{18}\text{O}]^+$ , which covered almost half of the glass surface in the interrogated regions and would be expected to block the glass substrate during the subsequent PDMS plasma bonding step. A comparison of the SIMS images of the control and plasma etched polystyrene samples is presented in Figure S4 of the electronic supplementary information. Oxygen plasma bonding of PDMS to glass relies on the formation of silanol groups on both surfaces; when the surfaces are brought together, the silanol groups condense, forming the permanent Si-O-Si (siloxane) bond<sup>38</sup>. As such, permanent oxygen plasma

1 bonding of PDMS is not feasible without reliable formation of  
 2 silanol groups on the glass surface. As the heavy alkoxyalkane-  
 3 like residual chemical species formed during the plasma  
 4 treatment (evidenced by the detection of the  $[C_8H_{18}O]^+$ ) would  
 5 block the surface during the plasma treatment and thus inhibit  
 6 formation of the silanol groups, it is likely that it may be the  
 7 chemical species responsible for the poor bonding performance  
 8 of glass surfaces after polystyrene plasma etch processes.

10 Although small amounts of  $[C_8H_{18}O]^+$  were also found on the  
 11 laser cut sample after bulk film lift-off, it covered less of the  
 12 surface, which enables more interfacial bonding between these  
 13 regions and PDMS. Furthermore, the SIMS image reveals that  
 14 two new chemical species were formed near the laser cut  
 15 regions of the laser-cut polystyrene-on-glass sample, which is  
 16 evidenced by the observation of the fragments  $[C_7H_6O_2Al]^+$  and  
 17  $[SnCH_3]^+$ . It is believed that the heat from the laser treatment  
 18 causes Sn and Al from the glass to react with the polystyrene,  
 19 as evidenced by the detection of  $[C_7H_6O_2Al]^+$  and  $[SnCH_3]^+$   
 20 peaks. Heightened levels of Sn and Al were also found on the  
 21 surface of a bare glass sample that had been treated with the  
 22 laser solely as compared to a degreased glass control. Although  
 23 these new chemical species have not been previously reported  
 24 in the literature to our knowledge, the formation of alkoxy  
 25 radicals in polystyrene layers under exposure to UV light (and  
 26 800 nm light from a femtosecond laser, hypothesized to be  
 27 under a multiphoton absorptive process) has been described in  
 28 the literature and attributed to photooxidation<sup>39-41</sup>. As these  
 29 new chemical species incorporate elements from both the glass  
 30 substrate and the polystyrene film, they could further improve  
 31 the adhesion of the polystyrene film near the pattern edges.  
 32 SIMS images of these fragments are presented in Figure S5 of  
 33 the electronic supplemental information.

34 ToF-SIMS analysis of the peeled-off region of the laser cut  
 35 sample immediately after a 1 minute 20 second exposure to air  
 36 plasma to simulate a plasma bonding process showed evidence  
 37 of heightened levels of  $[SiOH]^+$  and  $[SiOH_2]^+$  on the surface;  
 38 this result is similar to that observed for the degreased glass  
 39 control after the same plasma exposure. As these groups could  
 40 be involved in the formation of plasma bonds with silanol  
 41 groups on the PDMS surface, the presence of these ions  
 42 supports our observation that the peeled off region  
 43 demonstrates good ability to bond with PDMS. Relevant  
 44 regions of the ToF-SIMS spectra showing the effect of this  
 45 plasma exposure on the glass surface are included in Figure S5  
 46 of the electronic supplementary information.

47 The results obtained from the ToF-SIMS analysis indicate that  
 48 although oxygen plasma dry etch processes can remove the  
 49 polystyrene films, they leave behind a glass surface that is  
 50 contaminated with chemical species giving  $[C_8H_{18}O]^+$ . The  
 51 laser ablation process locally changes the glass surface  
 52 composition, as was evidenced by the detection of tin in these  
 53 regions. The focused UV laser not only ablated the polystyrene  
 54 film, separating patterned structures from the bulk, but also

55 melded the polystyrene with elements from the glass substrate  
 56 to form potentially useful adhesion components.

### Laser-patterned films function as oxygen sensors

57 Figure 4 (a) and (b) present the gaseous and fluidic calibration  
 58 of the oxygen sensors, respectively. The x-axis of Figure 4 (b)  
 59 represents the oxygen partial pressure in equilibrium with the  
 60 fluidic environment inside the chip, as the sensor itself was  
 inside a channel filled with water. The Stern-Volmer constants  
 obtained by fitting the calibration data to the Stern-Volmer  
 relationship ( $21 \text{ atm}^{-1}$  and  $11.8 \text{ atm}^{-1}$ , for the gaseous and  
 fluidic calibration, respectively) are in line with those  
 previously measured by our group for un-patterned films.  
 Please note that the differences in  $K_{SV}$  values for the fluidic  
 and gaseous cases can be attributed to concentration of quenching  
 species in the gaseous vs. dissolved environments at the same  
 partial pressure. Another contributing factor is differences in  
 the bimolecular rate constants ( $k_Q$  in Eq. 1) for the two  
 environments, which are in turn dependent on the diffusion  
 coefficients of oxygen (which changes with the media) and  
 fluorophore, as well as other factors<sup>42</sup>. No significant difference  
 was found between the datasets acquired at the lower flow rate  
 compared to those acquired at the higher flow rate. Analysis  
 of the images was performed in the same manner as for the  
 gaseous calibration. The errors on the datasets are largely due  
 to temporal variations in excitation source intensity; the use of  
 ratiometric sensors instead of the simple intensity-based sensors  
 used here would address this issue.

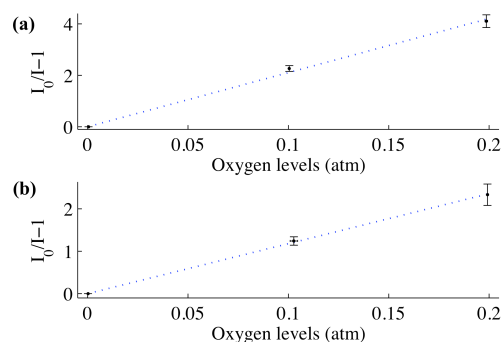


Figure 4. Results of (a) gaseous and (b) fluidic calibration of patterned oxygen sensors, along with a fit to the Stern-Volmer relationship. Error bars indicate one standard deviation bounds for the N=9 averaged datasets. Fit results yielded  $I_0=830\pm 100$  (gaseous) and  $610\pm 140$  (fluidic), and  $k_{SV}=21\pm 2 \text{ atm}^{-1}$  (gaseous) and  $11.8\pm 0.4 \text{ atm}^{-1}$  (fluidic).

### Laser-patterned sensors function during long-term perfusion flow

59 We did not observe sensor delamination within the device or  
 60 bubble generation in the fluid channels after the 3 day  
 experiment with the device immersed in fluid and with constant  
 gas and fluid perfusion. In separate tests, we tested the devices  
 with microfluidic flows resulting in shear rates of  $7.6 \text{ s}^{-1}$  up to  
 $15\,000 \text{ s}^{-1}$ , for periods of several hours to 3 days, and found the  
 sensors remained attached to the substrate. These results  
 indicate that the sensor patterning process yields sensors with

film adhesion compatible with multi-day microfluidic experiments. It also affirms that the glass-PDMS bond strength after our patterning method is sufficiently high for reliable microfluidic integration.

Figure 5 presents the results of an oxygen gradient measurement within the microfluidic gradient generator device. Figure 5 (a) shows the schematic of the gradient generator device along with the locations of the patterned sensors integrated within it, while (b) shows various sensor images and oxygen gradient maps taken using the fourth sensor from the device inlet (i-v). (i) shows the original phosphorescence intensity image taken during the calibration, with the channel filled with deoxygenated fluid. (ii) and (iii) show similar images of the sensor but under oxygen gradient conditions within the device, with oxygen and nitrogen supplied to the two gas control channels of the gradient generator device. In (ii), nitrogen was supplied to the left gas control channel and oxygen supplied to the right, while the gas inputs were switched for (iii). Finally, (iv) and (v) show a map of the dissolved oxygen levels obtained using the sensor intensities from (ii) and (iii), respectively, and the calibration data from Figure 4 (b). As the sensor was in a fluidic environment, the oxygen scale again represents the partial pressure of oxygen in a gaseous state that would be in equilibrium with the fluid.

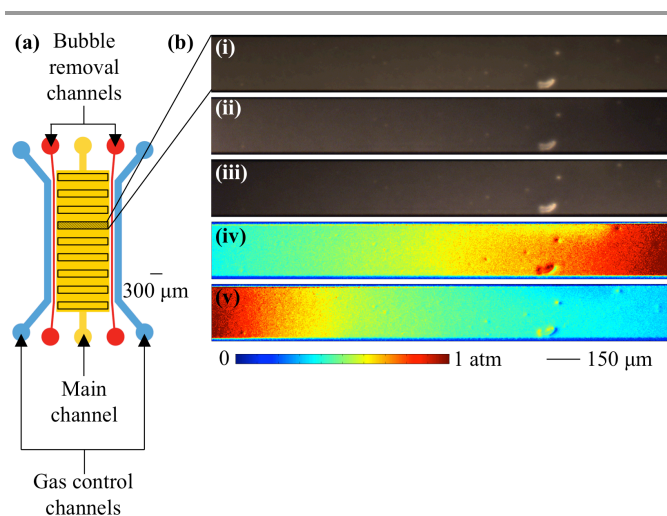


Figure 5. Dissolved oxygen measurements inside the gradient generator microfluidic device. (a) depicts the channel geometry of the microfluidic gradient generator, along with the positions of the patterned sensors integrated within it (shown by the black rectangles). (b) shows various sensor images and fluidic oxygen gradient measurements taken from the fourth sensor from the gradient generator device inlet. (i) shows the original image taken with the channel filled with deoxygenated fluid, yielding the reference  $I_0$ . (ii) shows the original sensor images taken with nitrogen supplied to the left gas control channel and oxygen supplied to the right. (iii) shows the original sensor image taken with oxygen supplied to the left gas control channel and nitrogen supplied to the right. (iv) and (v) show the oxygen levels obtained by analysing the intensities of (ii) and (iii), respectively.

These results demonstrate that the patterned sensors fabricated using the laser cutting method can be integrated into PDMS microfluidic devices using standard plasma bonding and exhibit

sufficient adhesion to the glass substrate to be compatible with many lab on a chip applications with incubation periods of days.

## Conclusions

We have developed a simple, mask-less, non-photolithographic method of patterning oxygen-sensitive polystyrene thin films, using laser ablation and aqueous lift-off of the bulk film. Feature sizes of 50  $\mu\text{m}$  on a 65  $\mu\text{m}$  pitch have been demonstrated using a 5  $\mu\text{m}$  laser beam. Unlike structures patterned with dry etch processes, structures patterned with our method can be easily integrated with PDMS microfluidic devices via standard plasma bonding. The method is fast, simple, and ideal for rapid prototyping due to its mask-less nature. Using AFM and ToF-SIMS analysis of the patterned samples, we found a combination of physical effects (breaking the polystyrene film without delamination) and chemical products of the photothermal ablation that could facilitate the patterning method. We analysed the chemical effects of laser and plasma treatments on polystyrene films using ToF-SIMS and detected  $[\text{C}_8\text{H}_{18}\text{O}]^+$  in the plasma etched regions, which likely indicates a heavy alkoxyalkane-like residual chemical species blocking the glass surface, inhibiting subsequent plasma bonding of PDMS. We also detected  $[\text{C}_7\text{H}_6\text{O}_2\text{Al}]^+$  and  $[\text{SnCH}_3]^+$  fragments in the laser cut regions, which are likely evidence of chemical compounds formed during the laser cutting process that could contribute to improved polystyrene-glass adhesion.

Sensors patterned with this method were integrated with a microfluidic device, calibrated, and used to measure gradients in dissolved oxygen levels within a PDMS microfluidic device; we found that the sensor adhesion and the PDMS-substrate bond strength were hydrolytically stable and sufficient for multi-day experiments in fluid.

Future work on this method will involve using the method to pattern ratiometric oxygen-sensitive films as well as integrating the resulting sensors into microfluidic cell culture environments. There may also be other applications for the patterning process beyond oxygen sensing; for example, polystyrene thin film ammonia<sup>43</sup> sensors could also potentially be patterned using this method.

## Acknowledgements

This work was carried out in the AMPEL Nanofabrication Facility along with the Interface Analysis and Reactivity Laboratory (IARL). We would like to acknowledge CMC microsystems for the provision of products and services that facilitated this research, including CAD design tools and fabrication assistance funding. The authors also gratefully acknowledge the Natural Sciences and Engineering Research Council of Canada (NSERC), the Canadian Breast Cancer

Foundation (CBCF), and the Canadian Institutes of Health Research (CIHR) for graduate and project funding.

## Notes and references

Electronic Supplementary Information (ESI) available: Supplementary figure S1 provides further details regarding the minimum spacing investigation. Supplementary figures S2-S3 provide AFM data regarding roughness and cross-sectional edge profiles. Supplementary figures S4-S5 provide ToF-SIMS ion images of the plasma etched and laser cut films. See DOI: 10.1039/b000000x/

1. S. M. Grist, L. Chrostowski and K. C. Cheung, *Sensors-Basel*, 2010, 10, 9286-9316.
2. A. Mills, *Platinum Metals Review*, 1997, 41, 115-127.
3. S. Suresh, V. C. Srivastava and I. M. Mishra, *Journal of Chemical Technology & Biotechnology*, 2009, 84, 1091-1103.
4. O. Stern and M. Volmer, *Phys Z*, 1919, 20, 183-188.
5. J. N. Demas, B. A. DeGraff and P. B. Coleman, *Anal Chem*, 1999, 71, 793A-800A.
6. P. Hartmann, W. Ziegler, G. Holst and D. W. Lubbers, *Sensor Actuat B-Chem*, 1997, 38, 110-115.
7. J. M. Vanderkooi, G. Maniara, T. J. Green and D. F. Wilson, *J Biol Chem*, 1987, 262, 5476-5482.
8. H. Xu, J. W. Aylott, R. Kopelman, T. J. Miller and M. A. Philbert, *Analytical Chemistry*, 2001, 73, 4124-4133.
9. E. J. Park, K. R. Reid, W. Tang, R. T. Kennedy and R. Kopelman, *J. Mater. Chem.*, 2005, 15, 2913-2919.
10. P. J. Cywinski, A. J. Moro, S. E. Stanca, C. Biskup and G. J. Mohr, *Sensor Actuat B-Chem*, 2009, 135, 472-477.
11. B. Ungerbock, V. Charwat, P. Ertl and T. Mayr, *Lab on a chip*, 2013, 13, 1593-1601.
12. Y. Amao, *Microchimica Acta*, 2003, 143, 1-12.
13. D. B. Papkovsky, G. V. Ponomarev, W. Trettnak and P. O'Leary, *Analytical Chemistry*, 1995, 67, 4112-4117.
14. A. P. Vollmer, R. F. Probst, R. Gilbert and T. Thorsen, *Lab on a chip*, 2005, 5, 1059-1066.
15. R. H. W. Lam, M.-C. Kim and T. Thorsen, presented in part at the Transducers & Eurosensors '07, Lyon, France, June 10-14, 2007, 2007.
16. R. H. Lam, M. C. Kim and T. Thorsen, *Analytical Chemistry*, 2009, 81, 5918-5924.
17. V. Nock, R. J. Blaikie and T. David, *Lab on a chip*, 2008, 8, 1300-1307.
18. V. Sunkara, D. K. Park, H. Hwang, R. Chantiwas, S. A. Soper and Y. K. Cho, *Lab on a chip*, 2011, 11, 962-965.
19. L. Tang and N. Y. Lee, *Lab on a chip*, 2010, 10, 1274-1280.
20. B. Y. Xu, X. N. Yan, J. J. Xu and H. Y. Chen, *Biomicrofluidics*, 2012, 6.
21. E. Sinkala and D. T. Eddington, *Lab Chip*, 2010, 10, 3291-3295.
22. H. X. Zhu, Y. Q. Tian, S. Bhushan, F. Y. Su and D. R. Meldrum, *Ieee Sensor*, 2010, 2053-2056.
23. R. Ambekar, J. Park, D. B. Henthorn and C.-S. Kim, *IEEE sensors journal*, 2009, 9, 169-175.
24. V. Nock, L. M. Murray, M. M. Alkaiji and R. J. Blaikie, 2010.
25. V. Nock, M. Alkaiji and R. J. Blaikie, *Microelectron. Eng.*, 2010, 87, 814-816.
26. S. M. Grist, L. Chrostowski and K. C. Cheung, presented in part at the The 16th International Conference on Miniaturized Systems for Chemistry and Life Sciences, Okinawa, Japan, October 29, 2012, 2012.
27. D. R. Day and S. D. Senturia, *J Electron Mater*, 1982, 11, 441-452.
28. Z. J. Yao, S. Chen, S. Eshelman, D. Denniston and C. Goldsmith, *J Microelectromech S*, 1999, 8, 129-134.
29. M. Tsunekawa, S. Nishio and H. Sato, *Jpn J Appl Phys I*, 1995, 34, 218-225.
30. M. Tsunekawa, S. Nishio and H. Sato, *J Appl Phys*, 1994, 76, 5598-5600.
31. M. A. Hopcroft, MPhil PhD Thesis, Cambridge University, 2002.
32. S. R. I. Gabran, R. R. Mansour and M. M. A. Salama, *Optics and Lasers in Engineering*, 2012, 50, 710-716.
33. L. Wang, W. M. Liu, Y. L. Wang, J. C. Wang, Q. Tu, R. Liu and J. Y. Wang, *Lab on a chip*, 2013, 13, 695-705.
34. P. C. Thomas, S. R. Raghavan and S. P. Forry, *Analytical Chemistry*, 2011, 83, 8821-8824.
35. Y. A. Chen, A. D. King, H. C. Shih, C. C. Peng, C. Y. Wu, W. H. Liao and Y. C. Tung, *Lab on a chip*, 2011, 11, 3626-3633.
36. D. K. Wood, A. Soriano, L. Mahadevan, J. M. Higgins and S. N. Bhatia, *Sci Transl Med*, 2012, 4.
37. R. S. Martin, A. J. Gawron and S. M. Lunte, *Anal Chem*, 2000, 72, 3196-3202.
38. S. Bhattacharya, A. Datta, J. M. Berg and S. Gangopadhyay, *J Microelectromech S*, 2005, 14, 590-597.
39. T. Ubukata, Y. Moriya and Y. Yokoyama, *Polym J*, 2012, 44, 966-972.
40. L. N. D. Kallepalli, S. V. Rao and N. R. Desai, *Opt Eng*, 2012, 51.
41. E. Yousif and R. Haddad, *SpringerPlus: Chemistry and Materials Science*, 2013, 2, 398.
42. J. R. Lakowicz and G. Weber, *Biochemistry-U.S.*, 1973, 12, 4161-4170.
43. H. S. Mader and O. S. Wolfbeis, *Analytical Chemistry*, 2010, 82, 5002-5004.